ACS APPLIED ENERGY MATERIALS

www.acsaem.org

Article

Experimental and Theoretical Optimization of Wearable Thermoelectric Generators Based on Fill Factor and Leg Geometry

Jeong Hun Kim,* Aminu Yusuf, Seung Eon Moon, Jong Pil Im, and Sedat Ballikaya*

Cite This: ACS Appl. Energy Mater. 2024, 7, 9315−9326

Read Online

ACCESS | Metrics & More | Article Recommendations | Supporting Information

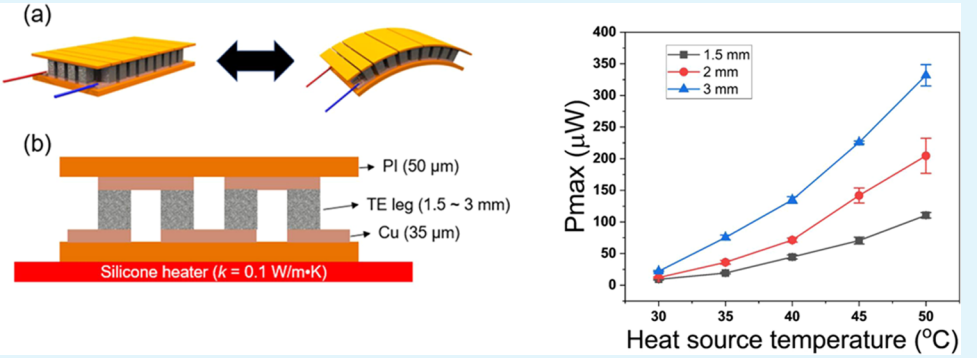

ABSTRACT: Conventional thermoelectric generators (TEGs) often exhibit low energy conversion efficiency, attributed to the subpar performance of thermoelectric (TE) materials and elevated contact resistance. Furthermore, structural inconsistencies may contribute to the diminished output performance. This report presents a theoretical analysis of wearable thermoelectric generators (TEGs), with experimental validation. Key findings include the necessity of electrical impedance matching to achieve maximum output power in a TEG. The open-circuit voltage of a TEG exhibits an increase with the number of thermocouples/fill factor, impacting the output power, which, in turn, depends on internal resistance and thermal resistance. Experimental results revealed the optimal leg lengths of 1.5 and 3 mm for TE modules with 31-pair and 40-pair at a fixed temperature gradient. At a 9 K temperature gradient for the 31-pair TE module, maximum output powers of 1596, 1382, and 932 μW were obtained when the leg lengths were 1.5, 2, and 3 mm, respectively. The report also highlights the influence of leg length on output power for both flat and curved heat sources (50 °C), with the highest output powers recorded at 313.9 and 331.9 μW for the TE module with 31-pair and L = 3 mm. These insights contribute to the understanding and optimization of wearable TEGs for enhanced performance.

KEYWORDS: *energy harvesting, fill factor, maximum power, optimum parameters, thermoelectric generator, wearable applications*

1. INTRODUCTION

Thermoelectric generators (TEGs) have been attracting researchers' attention due to their ability to directly convert heat energy into electrical energy. Additionally, their characteristics, such as flexibility, noiseless operation, lightweight, mechanical stability, long life span, zero emissions, and 24 h operation, make them excellent candidates for wearable applications. It is known that humans constantly generate thermal energy due to metabolism; a wearable thermoelectric generator (w-TEG) worn on a human body can convert the temperature difference between the human body and the surroundings into electrical energy for wearable applications.[1] The output powers of TEGs are generally low, vary with temperature gradient and other environmental conditions, and thus are not suitable for direct use in powering electronic devices. For proper operation, an energy management circuit needs to be integrated with the TEGs to power electronic devices.[2] The energy management circuit stabilizes and boosts the output voltage of the TEGs, where most of the time, a maximum power point tracking algorithm is employed. Several studies have demonstrated various applications of w-TEGs, which include powering an electronic calculator,[3,4] light-emitting diode (LED),[5,6] temperature- and humidity-monitoring device,[7] watch,[8,9] accelerometer,[10] etc.

During the fabrication and characterization of flexible TEGs, researchers often ensure that the TEGs are mechanically stable and can return to their original form after bending or stretching. Bending cycle tests should also be carried out to determine the variation of the internal resistance with the number of bending. Ideally, the internal resistance should

Received: July 11, 2024
Revised: September 21, 2024
Accepted: September 23, 2024
Published: October 7, 2024

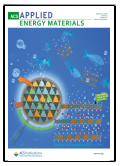

remain constant with the variation in the number of bendings; however, this is not usually the case. Even the most flexible TEG can have a small variation in its internal resistance. The flexible TEGs can be in either a cross-plane or an in-plane configuration. TE legs in an in-plane configuration lie in the same plane as the heat source. To create a temperature gradient, heat absorption on one side of the flexible TEG is enhanced and heat dissipation is also enhanced on the other side. In-plane flexible TEGs are usually preferred in wearable applications because of their simple structure, ease of fabrication, and excellent mechanical stability upon large twisting deformation or mechanical bending.[11,12] Additionally, in-plane flexible TEGs can be made junction-free and thereby have no junction losses, which are present in conventional TEGs.[13] Liang et al.[14] developed an in-plane flexible TEG using silver chalcogenide foils as the n-type leg and copper as the p-type leg. The developed flexible TEG generated an open-circuit voltage of 1.19 mV and an output power density of 1.8 mW m^{-2} at a temperature gradient of 2.7 °C. Lee et al.[15] reported a free-standing/substrate-free Ag_2Se film's flexible TEG. The zT of the Ag_2Se films was measured to be 0.514 ± 0.060 at room temperature. The substrate-free films exhibited superior flexibility compared with the films constrained on a substrate. Palaporn et al.[16] fabricated a flexible paper TEG using bacterial cellulose/silver selenide (BC/Ag_2Se) nanocomposites. The study reveals the power factor, thermal conductivity, and zT of 642 μW m^{-1} K^{-2}, 0.36 Wm^{-1} K^{-1}, and 0.70 at 400 K, respectively. The fabrication process of the BC/Ag_2Se paper is scalable and does not require the use of advanced/expensive equipment. Another significant development in the field of energy harvesting is self-healing flexible TEGs.[17] The device can heal itself after fracture simply by moisturizing and bringing the two ends in contact with one another. The study showed that the ternary composite poly(3,4-ethylene-dioxythiophene)/poly(styrenesulfonate) (PEDOT/PSS) possesses a healing ability of 78%. The resistance of the healed composite material increases by only 26.62% compared to that of the original film, suggesting good electrical stability after self-healing.

Creating a large temperature gradient across the hot and cold sides of an in-plane flexible TEG is challenging because both the hot and cold sides are in contact with the heat source. This is one of the reasons why flexible TEGs made up of thin films have lower performance compared to that of cross-plane flexible TEGs. You et al.[18] presented a cross-plane flexible polyimide TEG with one side cut into blocks to allow the TEG to achieve a bending radius of 4.5 mm. At a temperature gradient of 50 K, the TEG generated an open-circuit voltage and output power of 236 mV and 4.19 mW, respectively. The output performance shows an insignificant change after 7400 times of bending cycles, indicating high thermo-mechanical stability. Xu et al.[19] developed a mushroom-shaped flexible TEG through a low-cost fabrication process. TE legs are sandwiched between copper electrodes that enable heat absorption and dissipation, and a fabric is included to add comfort and prevent heat leakage. When worn on the forehead, the flexible TEG has produced a maximum output power density of 48 mW/cm^2 at an ambient temperature of 15 °C and a wind speed of 2 m/s. The device is also able to illuminate a reading lamp consisting of light-emitting diodes for reading at night. Zhang et al.[20] reported a lightweight, high-power flexible μTEG, which was fabricated via pulse electroplating. The μTEG was optimized by tuning the electroplating conditions of TE legs. The μTEG exhibits a device-level voltage factor, power factor, and normalized power-to-weight ratio of 65.2 mV cm^{-2} K^{-1}, 16 μW cm^{-2} K^{-2}, and 212 μW g^{1-} K^{-2}, respectively. To maintain a substantial temperature difference between the two sides of the flexible TEG, Hasan et al.[21] developed a vertically aligned poly(3,4-ethylene-dioxythiophene)/poly(styrenesulfonate) (PEDOT/PSS) thin film (p-type) and aluminum wire-based (n-type) flexible TEG. When worn on the wrist, the device generated an open-circuit voltage of 1.46 mV. When operated at a temperature difference of 80 °C, it generated a maximum output power of ∼2.4 nW and an output power density of 1.5 nW cm^{-2}. To improve the heat dissipation of a flexible TEG, a heteromorphic electrode (heat sink plus electrode) was applied to the cold side of the TEG. The heteromorphic electrode enhances the output power by 44.1 times compared to conventional electrodes.[22] A novel TEG that simultaneously absorbs heat and light has also been demonstrated by Jeong et al.[23] A printable solar-absorbing layer with an absorptivity of 95% was placed on the hot side of a wearable TEG; this layer converted solar energy into thermal energy. The TEG utilizes both solar energy and heat energy from the human body. Despite all attempts to provide vertical temperature gradients for thin film wearable TEGs, the low electrical conductivity, due to grain boundary scattering, makes their performance lower than that of wearable TEGs made up of ingot TE materials. This is one of the reasons that compel researchers to retain ingot TE materials for wearable TEGs.

The fill factor (FF), which is the ratio of the actual area covered by the TE material to that of the substrate, also plays an important role in determining the output performance of a w-TEG. If the FF is very small ($\ll$1), a filler material needs to be used to fill up the void for mechanical support.[24] The thermal conductivity of the filler material should be as minimal as possible to minimize parasitic heat losses. Commonly used filler materials include aerogel, polyimide, and PDMS. Among these materials, aerogel has the least thermal conductivity and is therefore an excellent filler material. Due to the aforementioned reason, TE modules with no filler material (air between the TE legs) have higher performance than TE modules with polyurethane foam/PDMS.[25] A three-dimensional (3D) computational parametric study shows that the value of the optimal FF increases with an increase in either the TE leg length or the area of external heat spreaders.[26] Other factors that affect the performance of w-TEGs are ambient temperature and air velocity.[27] The w-TEG would continue to produce output power if the ambient temperature is not equal to the body temperature. It is often desired that the ambient temperature be lower than the body temperature for heat to be dissipated from the cold side to the surroundings. Conversely, an increase in air velocity enhances the output power due to the increase in the heat rejection from the cold side; however, the heat rejection saturates at some high velocities. The increase in air velocity will also increase parasitic losses if the w-TEG is not sealed and air is between the TE legs. In that case, both parasitic losses and performance enhancement due to convective heat transfer on the cold side should be considered simultaneously in the design of a w-TEG with no filler material. A single-objective or multiobjective optimization technique can also be used to determine the optimum FF of the w-TEG for enhancing the power output.[28,29] For single-objective optimization, parameters that the FF depends on, such as leg length, number of TE couples, area of the TE legs,

https://doi.org/10.1021/acsaem.4c01794
ACS Appl. Energy Mater. 2024, 7, 9315−9326

convective heat transfer coefficient, and hot and cold side thermal resistances, can be concurrently varied until an optimum output power/energy conversion efficiency is found. For multiobjective optimization, the goal will be to find a trade-off between two or more conflicting objective functions. This technique is efficient and faster than single-parameter optimization. After the output power has been generated by the TEG, its output power needs to be transferred efficiently to the load efficiently. Due to the variation of the output voltage of a TEG with temperature, a DC−DC converter is usually connected between the TEG and the electrical load to ensure stable and continuous energy supply.[30] The choice of a suitable DC−DC converter among the buck, boost, and buck-boost converters depends on the electrical output and the load requirements. In many cases, the buck-boost DC−DC converter is preferred because it can operate when the output voltage of the TEG is lower or higher than the required load voltage. To maximize the output power, an MPPT algorithm can be used to continuously track the output voltage of the TEG by adjusting the duty cycle of the converter to match the required output voltage.[31]

While there has been considerable research dedicated to TEGs for wearable applications, the geometric optimization of flexible TEGs without filler material has been notably absent from prior studies. Recognizing this research gap, the present study aims to address this void in the literature by conducting a comprehensive investigation. The theoretical exploration delves into the impact of various parameters, including fill factor, leg length, thermal conductivity of the material, and shape of the heat source, on the output performance of wearable TEGs. Through a systematic theoretical analysis, the study seeks to provide valuable insights into the intricate relationships between these parameters and the overall effectiveness of flexible TEGs. Subsequently, the theoretical findings are subjected to experimental validation, adding a crucial empirical dimension to the research. This multifaceted approach contributes to advancing the understanding of flexible TEGs, shedding light on key design considerations, and paving the way for the development of more efficient and optimized wearable energy harvesting devices.

2. MATHEMATICAL MODEL

The w-TEGs presented in this study are composed of n- and p-type TE legs arranged thermally in parallel and electrically in series, printed on flexible polyimide substrates, as shown in Figure 1a,b. Although using filler material between the legs provides mechanical support to the w-TEG, parasitic losses are present due to heat transfer through the filler material. Since the thermal conductivity of commonly used filler materials is higher than that of air, parasitic losses can be reduced when no filler material is used.

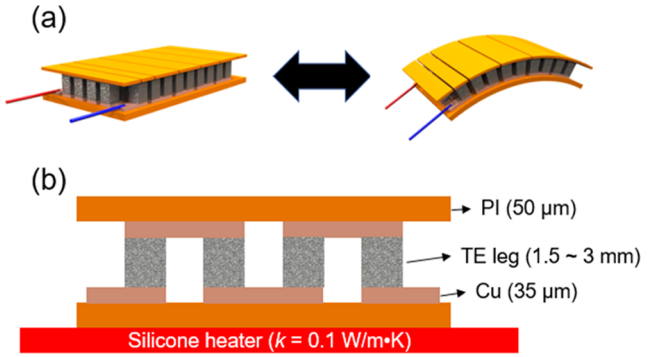

Figure 1. (a) 3D Of the geometry of the proposed flexible TEG and (b) 2D dimension of the proposed flexible TEG.

Based on one-dimensional energy analysis, the heat absorbed by the hot side and heat released from the cold side are, respectively, given as[32]

$$Q_h = N\left[S_h T_h I - \frac{1}{2}I^2 R_i - \frac{1}{2}\tau I(T_h - T_c) + \frac{1}{R_{TE}}(T_h - T_c)\right] \quad (1)$$

$$Q_c = N\left[S_c T_c I + \frac{1}{2}I^2 R_i + \frac{1}{2}\tau I(T_h - T_c) + \frac{1}{R_{TE}}(T_h - T_c)\right] \quad (2)$$

where N is the number of TE couples, S is the Seebeck coefficient, I is the electric current, R_i is the internal resistance, T is the temperature, τ is the Thomson coefficient, and subscripts c and h refer to the cold and hot sides, respectively.

The electrical output power can be obtained by subtracting eq 2 from eq 1

$$P_{TE} = N[(S_h T_h - S_c T_c)I - I^2 R - \tau I(T_h - T_c)] \quad (3)$$

where the first term in the bracket represents the Peltier power, the middle term is the Joule heat, and the last term is the Thomson effect. For wearable applications, TEGs are not subjected to a large temperature gradient; as such, average TE properties can be used to analyze the performance of the devices. In that sense, the small Thomson coefficient can be neglected. Hence, the output power given in terms of the load resistance can be expressed as

$$P_{TE} = \left[\frac{N\, S_{av}(T_h - T_c)}{R_i + R_L}\right]^2 R_L \quad (4)$$

where S_{av} is the average Seebeck coefficient and R_i is the total internal resistance given as

$$R_i = \frac{N l_p}{\sigma_p A_p} + \frac{N l_n}{\sigma_n A_n} + R_{ele} \quad (5)$$

where l is the leg length, A is the cross-sectional area of the TE leg, R_{ele} is the total resistance of copper electrodes, and n and p refer to the n- and p-type TE materials, respectively. Likewise, the thermal resistance of the TE legs is given as

$$R_{TE} = \frac{l}{N(A_n k_n + A_p k_p)} \quad (6)$$

where k is the thermal conductivity of the material.

Now, the FF of the device is

$$FF = \frac{A_{TE}}{A_{TEG}} \quad (7)$$

where A_{TEG} is the external surface area of the w-TEG and A_{TE} is the total area covered by the TE legs and is defined as

$$A_{TE} = 2NA_{n/p} \quad (8)$$

Eqs 5 and 6 can be given in terms of the FF as

https://doi.org/10.1021/acsaem.4c01794
ACS Appl. Energy Mater. 2024, 7, 9315−9326

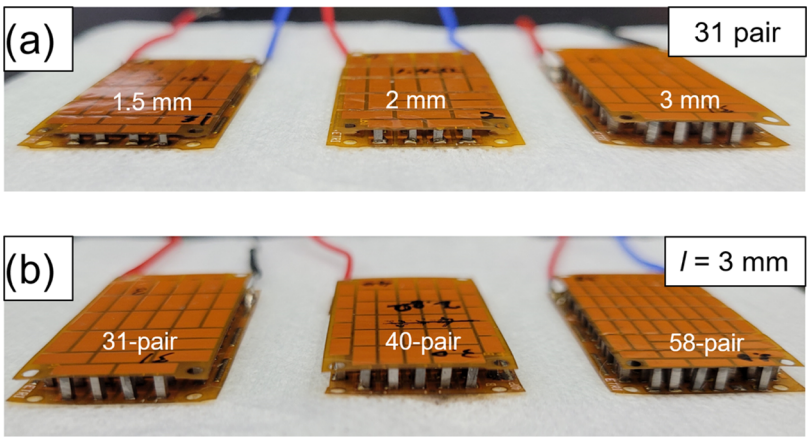

Figure 2. Fabricated modules with (a) different leg lengths and (b) different numbers of thermocouples.

$$R_i = \frac{2N^2 l}{A_{TEG}FF}\left(\frac{\sigma_n + \sigma_p}{\sigma_n \sigma_p}\right) + R_{ele} \tag{9}$$

$$R_{TE} = \frac{2l}{A_{TEG}FF(k_p + k_n)} \tag{10}$$

Substituting eq 9 into eq 4, one can obtain the output power as

$$P_{TE} = \left[\frac{N\, S_{av} FF A_{TEG} \sigma_n \sigma_p (T_h - T_c)}{2N^2 l(\sigma_n + \sigma_p) + A_{TEG}FF\sigma_n\sigma_p(R_{ele} + R_L)}\right]^2 R_L \tag{11}$$

It can be seen that the output power and leg length have a simple relationship. On the other hand, the relationship between the output power and the FF is complex; thus, a parametric study can determine this parameter's influence on the output power. Equation 11 gives the output power when the thermal and electrical contact resistances are assumed to be negligible. However, when the thermal contact resistances are to be considered, the w-TEG can be modeled by a voltage source and an equivalent Thevenin resistance in series, and they are respectively given as[33]

$$V_{Eq} = \frac{N\, S_{av} R_{TE}\, (T_s - T_a)}{R_{TE} + 2R_s} \tag{12}$$

Table 1. Properties of the Materials Used

material	ρ_d (g/cm^3)	S (μV K^{-1})	k (Wm^{-1} K^{-1})	σ (S m^{-1})
$Bi_2Se_{0.2}Te_{2.8}$	7.83	−203.06	2.01	1.33×10^5
$Sb_{1.5}Bi_{0.5}Te_3$	6.81	204.98	1.86	1.25×10^5
copper	8.93		385	5.9×10^7
colder	7.24		55	2×10^7
PI film	1.42		0.15	

$$R_{Eq} = R_i + \frac{N\, S_{av}^2 R_{TE} R_s\, (T_s - T_a)}{R_{TE} + 2R_s} + R_{con} \tag{13}$$

where T_a is the ambient temperature, R_s is the thermal resistance of the substrate, T_s is the heat source temperature, and R_{con} is the contact resistance at the interfaces and is assumed to be 10% of the R_i. The thermal resistances of the substrate can be calculated from

$$R_s = \frac{l_s}{A_s\, k_s} \tag{14}$$

where l_s is the thickness of the material, and A_s and k_s are the substrate's surface area and thermal conductivity, respectively.

The output power supplied to the load, considering the impact of thermal and contact resistances, can be determined from eqs 12 and 13 as

$$P_{TE} = \left[\frac{N\, R_{TE}\, S_{av}\, FF\, A_{TEG}\, \sigma_n\, \sigma_p\, (T_s - T_a)}{2N^2 l(\sigma_n + \sigma_p)[R_{TE} + 2R_s] + NA_{TEG}\, S_{av}^2\, R_{TE}\, R_s\, FF\, \sigma_n\, \sigma_p\, (T_s - T_a) + M[R_{ele} + R_{con} + R_L]}\right]^2 R_L \tag{15}$$

where $M = A_{TEG}\, FF\, \sigma_n\, \sigma_p[R_{TE} + 2R_s]$

3. EXPERIMENTAL SECTION

3.1. Fabrication of Thermoelectric Module. Printed circuit boards (PCBs) were fabricated on the polyimide (PI) film substrate for the thermoelectric modules. They were composed of 31, 40, and 58 pairs of n-type and p-type thermoelectric legs (Livingcare, Korea) through the top and bottom PCBs. First, solder paste (SAC305, Tamura, Japan) was printed onto the PCB by the screen-printing method. Thermoelectric legs were assembled on the bottom PCB through a metal jig and bonded by heat treatment in a convection oven (250 °C, 10 min). After removal of the jig, the attached TEG legs were aligned to the top PCB followed by the same heat treatment. Six different TE modules with no filler material between the TE legs were fabricated as shown in Figure 2, and the properties of the materials are given in Table 1.

3.2. Measurement of the Output Performance of the TE Modules. The internal resistance and z ($1/K$) values of each TE module were measured as given in Table 2. Thereafter, the open-circuit voltage and the maximum output power were measured using a source meter (KEITHELY 2401). All measurements were performed after sufficient time had elapsed for the voltage to stabilize. The performance of each TE module was examined through three different experimental setups, as shown in Figure 3. Forced water cooling (Figure 3a) was achieved by creating fixed temperature gradients across the two sides of the TE modules. Figure 3b shows the setup where the TE module is placed on a flat silicone heater via a thermal pad. Likewise, Figure 3c presents the case where the TE module is placed on a curved silicone heat source with a radius of 4 cm. In both

https://doi.org/10.1021/acsaem.4c01794
ACS Appl. Energy Mater. 2024, 7, 9315−9326

Table 2. Measured Z Value and Internal Resistance of the w-TEGs

parameter	31-pair 1.5 mm	31-pair 2 mm	31-pair 3 mm	40-pair 3 mm	58-pair 3 mm
Z value (Z-meter) × 10^{-3} (K^{-1})	0.548	0.554	0.533	0.589	0.675
internal resistance (Ω)	1.1	1.38	2.01	2.41	3.5
fill factor		0.078		0.101	0.146

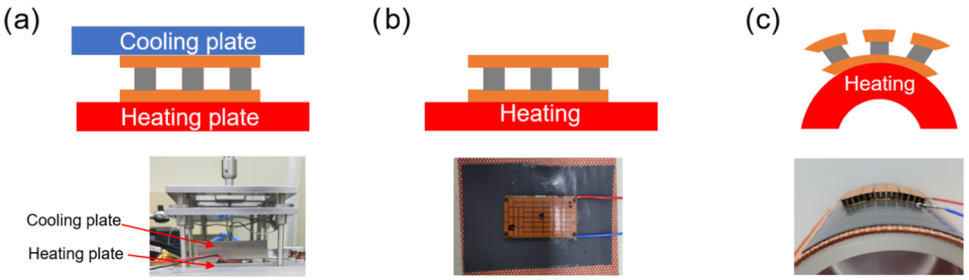

Figure 3. Experimental setup: (a) forced water cooling, (b) flat heat source, (c) curved heat source.

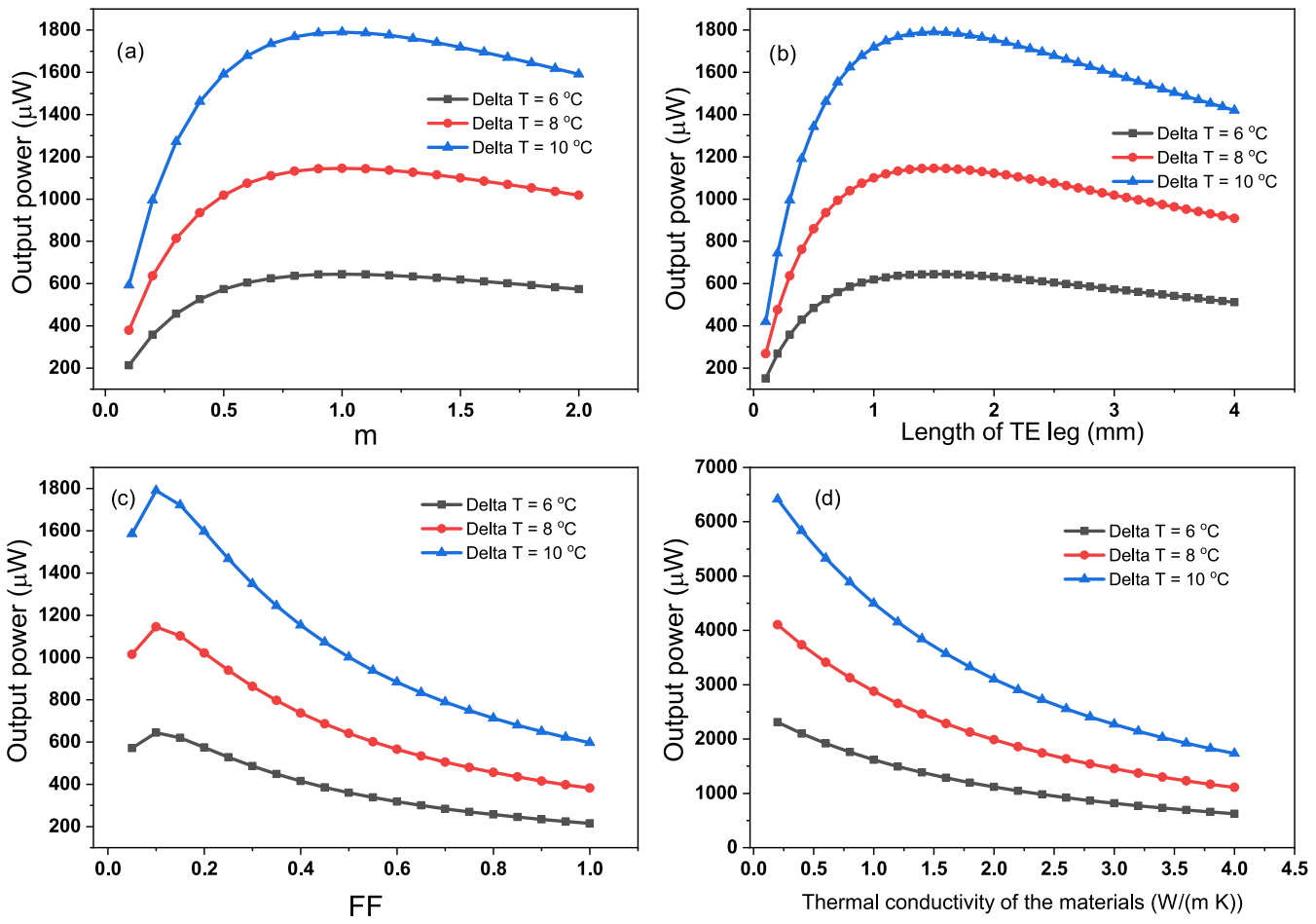

Figure 4. Variation of output power with (a) electrical impedance, (b) leg length, (c) fill factor, and (d) thermal conductivity of materials.

cases, the power generation performance was measured by increasing the temperature from 30 to 50 °C. The maximum power of the device was calculated from swept voltage−current data, repeated at least 3 times.

4. RESULTS AND DISCUSSION

4.1. Theoretical Analysis. It is widely believed that the TEG can deliver maximum power when the load resistance is matched with the internal resistance of the TEG. However, due to the Peltier and Joule effects, a TEG does not obey the maximum power transfer theorem. Thus, the maximum power occurs when the load resistance is $R_L = R_i\sqrt{1 + ZT}$, where R_i is the internal resistance and ZT is the dimensionless figure of merit of the device.[34] This is known as electrical impedance matching. Herein, the ratio of the load resistance to the internal resistance (m) was varied to determine its influence on the output power of the w-TEG. The analysis in this section was carried out considering the overall external dimension of the substrate as 22 mm × 36 mm, TE leg length of 1.5 mm, leg

https://doi.org/10.1021/acsaem.4c01794
ACS Appl. Energy Mater. 2024, 7, 9315−9326

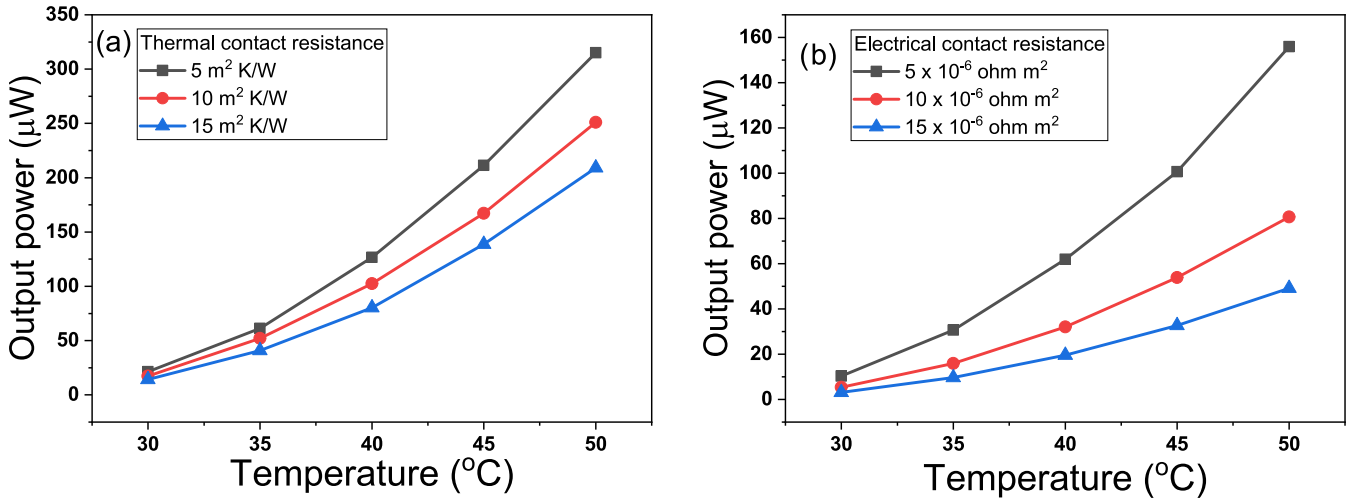

Figure 5. Effect of (a) thermal contact resistance on the output power and (b) electrical contact resistance on the output power.

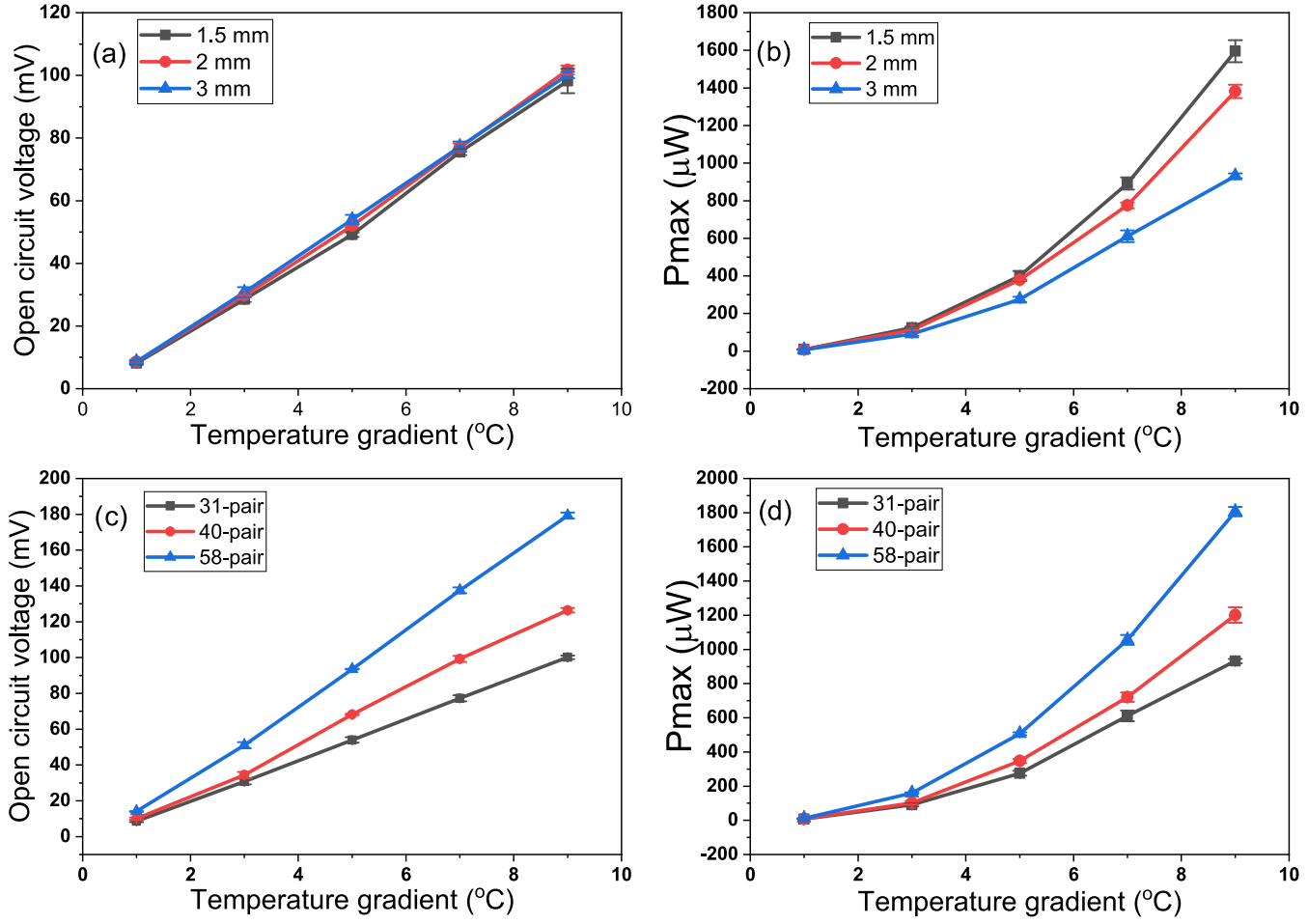

Figure 6. Forced water cooling: different heights of the TE legs (31-pair) (a) open-circuit voltage, (b) maximum output power; different filling factor (3 mm leg length), (c) open-circuit voltage, (d) maximum output power.

surface area of 1 mm × 1 mm, fill factor of 0.078, which correspond to 31-pair, and fixed temperature gradients ($T_h - T_c$) of 6, 8, and 10 °C, and that the thermal and electrical contact resistances are negligible (eq 11). In each of the three cases (Figure 4a), the output power increases and then decreases with an increase in the value of m. One can also observe that the higher the temperature gradient, the higher the output power. At the point of electrical impedance matching, the maximum powers were found to be 644, 1145, and 1790 μW at ΔT = 6, 8, and 10 °C, respectively.

Figure 4b shows the variation of output power with the length of the thermoelement. Similar to electrical impedance matching, the length of the thermoelement also plays a vital role in determining the maximum output power. Generally,

https://doi.org/10.1021/acsaem.4c01794
ACS Appl. Energy Mater. 2024, 7, 9315−9326

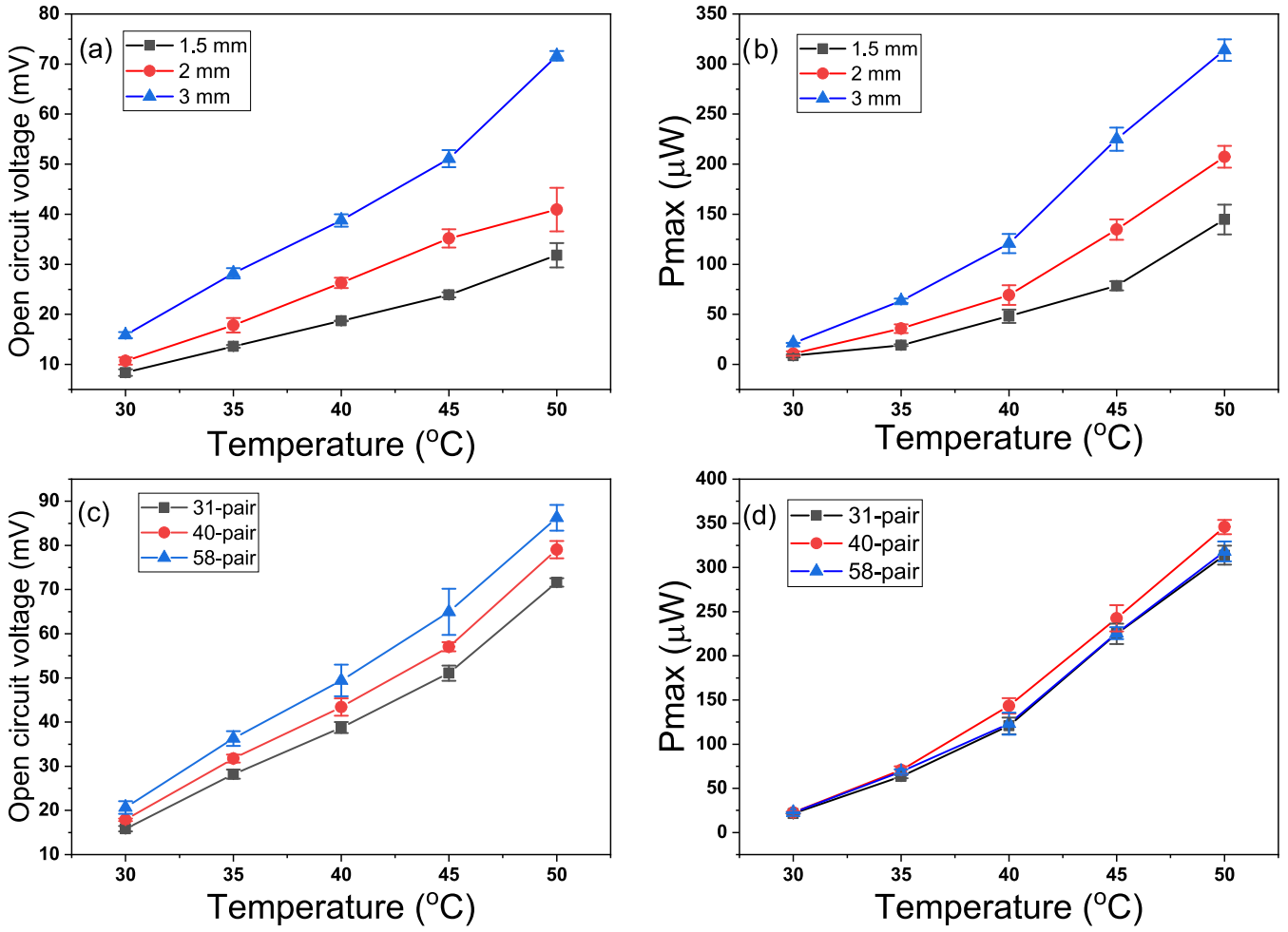

Figure 7. Flat heat source: different heights of the TE legs (31-pair) (a) open-circuit voltage, (b) maximum output power; different fill factor (3 mm leg length) (c) open-circuit voltage, (d) maximum output power.

longer thermoelements exhibit a larger temperature gradient due to higher thermal resistance compared to shorter thermoelements. Therefore, for transient analysis, w-TEGs made up of longer thermoelements are expected to demonstrate a higher output performance compared to w-TEGs with shorter thermoelements. However, at a fixed temperature gradient, the output power does not consistently increase with an increase in leg length. This is because the internal resistance increases with the leg length. The leg length was varied in a step size of 0.1 mm, from 0.1 to 4 mm. It can be seen that as the leg length increases from 0.1 to 1.5 mm, the output power increases. Upon exceeding the optimum leg length, the output power reduces with further increases in leg length. This is because of the negative effect of the internal resistance on the output power. It is also observed that higher temperature gradients lead to a higher output power. At the optimum leg length, which is L = 1.5 mm, the maximum powers are 645, 1150, and 1790 μW at the corresponding ΔT = 6, 8, and 10 °C, respectively.

The fill factor (FF) was varied from 0.1 to 0.99 to determine its influence on the power, as shown in Figure 4c. Increasing the FF causes an increase in the open-circuit voltage; however, the output power initially increases and then decreases due to the increase in the internal resistance of the TEG, and this shows that TEGs have an optimum FF. For the TE material considered in this study, with L = 1.5 mm, the optimum FF was found to be 0.078 (31-pair). Figure 4d presents the variation of the output power with the total thermal conductivity of the TE materials. At all temperature gradients, the output power decreases with an increase in the total thermal conductivity of the materials. This suggests that to achieve high output power, the thermal conductivity should be as low as possible.

The impact of thermal and electrical contact resistances on the output power (eq 15) of a 31-pair, L = 3 mm w-TEG is illustrated in Figure 5. This analysis is performed at an ambient temperature of 23 °C. In Figure 5a, it is evident that the output power increases with rising heat source temperature but decreases with increasing thermal contact resistance, indicating its negative impact on output power. Figure 5b shows how output power varies with the electrical contact resistance and heat source temperature. It is observed that a higher electrical contact resistance results in lower output power, whereas increasing the heat source temperature enhances the output power. A comparison of Figure 5a,b reveals that electrical contact resistance has a more adverse effect on output power than thermal contact resistance. For more efficient operation of the w-TEG, it is crucial to minimize both resistances.

4.2. Experimental Analysis. *4.2.1. Forced Water Cooling (Fixed Temperature Gradient).* Based on the theoretical analysis, the optimum leg length of 1.5 mm and FF of 0.078 (31 pairs) were determined. This provides a guide to narrow

https://doi.org/10.1021/acsaem.4c01794
ACS Appl. Energy Mater. 2024, 7, 9315−9326

the search for determining the actual optimum values experimentally. The variation of the environmental conditions during the operation of the TEG may shift the values of the optimum parameters; thus, TE modules with different TE leg lengths and fill factors were fabricated, as shown in Figure 2. The FFs and leg lengths are tailored to be around the optimum theoretical values. Analysis in Figure 5 was conducted based on the forced water cooling setup as given in Figure 3a. Temperature gradients from 1 to 9 °C were created, and the corresponding open-circuit voltage and output power were measured.

Figure 6a presents the variation of the open-circuit voltage with the temperature gradient for different leg lengths (see Appendix A for the interpretation of the error bars). The results show that the open-circuit voltage of the longer TE legs is slightly higher than that of the shorter TE legs. This confirms that the internal resistance does not influence the open-circuit voltage. As expected, the open-circuit voltages increase monotonically with an increase in the temperature gradient. The highest open-circuit voltages of 98.2, 101.7, and 100 mV were obtained at the leg lengths of 1.5, 2, and 3 mm, respectively. Variations of the output powers of the three w-TEGs with the temperature gradient are presented in Figure 6b. The output power also increases with an increase in the temperature gradient; however, the relationship between the output power and temperature is nonlinear. Even though the three TE modules have similar open-circuit voltages, the difference between the output powers of the three modules varies significantly. The output power increases with the decrease in the leg length due to the reduction in the internal resistance of the module. Moreover, this result shows that the leg length L = 1.5 mm is closer to the optimum leg length, which corresponds to the number of thermocouples of 31. This also confirms that the maximum output power depends on the relationship between leg length and the FF. At the maximum temperature gradient of 9 K, the highest output powers of 1596, 1382, and 932 μW were obtained at the leg lengths of 1.5, 2, and 3 mm, respectively.

Figure 6c presents the variation of the open-circuit voltages of the 31-pair (FF = 0.078), 40-pair (FF = 0.101), and 58-pair (FF = 0.147) TE modules with the variation of the temperature gradient at a leg length of 3 mm. In all cases, the open-circuit voltages linearly increase with an increase in the temperature gradient. As the FF increases, the energy absorption also increases, leading to an increase in the open-circuit voltage. The highest open-circuit voltages of 100.2, 126.4, and 179 mV were obtained when the number of thermocouples was 31, 40, and 58, respectively. It should be observed that the open-circuit voltages of the two cases (40-pair and 58-pair) in Figure 6c are higher than those in Figure 6a because of the increase in the number of thermocouples, resulting in higher voltage generation.

Figure 6d shows the output power of the three different numbers of thermocouples at a leg length of 3 mm. Like the open-circuit voltage, the output power also increases with the increase in the temperature gradient. The TE module with 58 pairs has the highest output power due to the highest energy absorption/utilization. At the maximum temperature gradient of 9 K, the highest output powers of 932, 1201, and 1806 μW were obtained for the N = 31, 40, and 58 pairs, respectively. The results indicated that for a leg length of 3 mm, the optimum FF is 0.147, which corresponds to 58 pairs. This validated the theoretical result that the optimum FF depends on the leg length.

4.2.2. Flat Heat Source. Figure 7 presents the module analysis based on a flat heat source. In each case, the hot side of the module was attached to the heat source, while the cold side was cooled by natural convection. The ambient temperature is 23 °C, and the heat source temperature increases from 30 to 50 °C at regular intervals of 5 °C. Figure 7a,b shows that both the open-circuit voltage and the output power increase with the rise in the heat source temperature. Similarly, both the open-circuit voltage and the output power increase with the increase in the leg length. The output power in Figure 7b increases with an increase in the leg length due to the increase in the temperature gradient, which is due to the increase in the thermal resistance. It should be noted that continuously increasing the leg length in an attempt to achieve higher output power might not be effective because, at a particular point, the effect of increasing the internal resistance will outweigh the increase in the temperature gradient. At the heat source temperature of 50 °C, the open-circuit voltages of 31.8, 40.9, and 71.6 mV were obtained when the leg lengths are 1.5, 2, and 3 mm, respectively. Likewise, their corresponding maximum output powers of 145, 207.4, and 314 μW were obtained. This demonstrates that the open-circuit voltages and output powers in Figure 7a,b are lower than those in Figure 6a,b due to the lower cooling performance in the former. Also, due to the absence of proper cooling on the cold side, the maximum output was not found at the optimum FF; rather, the output power shows an increasing trend with the increase in the leg length. This is because the temperature gradient increases with an increase in the leg length, which eventually increases the output power.

Figure 7c,d presents the open-circuit voltage and the output power of the 31-pair, 40-pair, and 58-pair TE modules with a leg length of 3 mm. The open-circuit voltage increases with the increase in both the number of thermocouples and the heat source temperature. An increase in the number of thermocouples increases energy absorption. It should be noted that the temperature gradient reduces with an increase in the number of thermocouples. The effect of the reduction in the temperature gradient is compensated by the increase in the number of thermocouples, leading to the increase in the open-circuit voltage with the increase in the number of thermocouples. On the other hand, the output power is proportional to the number of thermocouples and the square of the temperature gradient. This means that the effect of decreasing/increasing the temperature gradient on the output power can be higher or lower than the effect of increasing/decreasing the number of thermocouples. Thus, the 40-pair TE module is found to be superior to the other two modules. For 31-pair TE module, the effect of lowering the number of thermocouples is higher than the positive influence of increasing the temperature gradient on the output power. Meanwhile, for the 58-pair TE module, the effect of lowering the temperature gradient is higher than the positive influence of increasing the number of thermocouples on the output power. Hence, the output powers of the two TE modules are lower than that of the 40-pair TE module. At the heat source temperature of 50 °C, the open-circuit voltages of 71.6, 79, and 86.3 mV were obtained for the 31-pair, 40-pair, and 58-pair, respectively. The corresponding output powers are 314, 346, and 318.2 μW, respectively. The 40-pair TE module has the

https://doi.org/10.1021/acsaem.4c01794
ACS Appl. Energy Mater. 2024, 7, 9315−9326

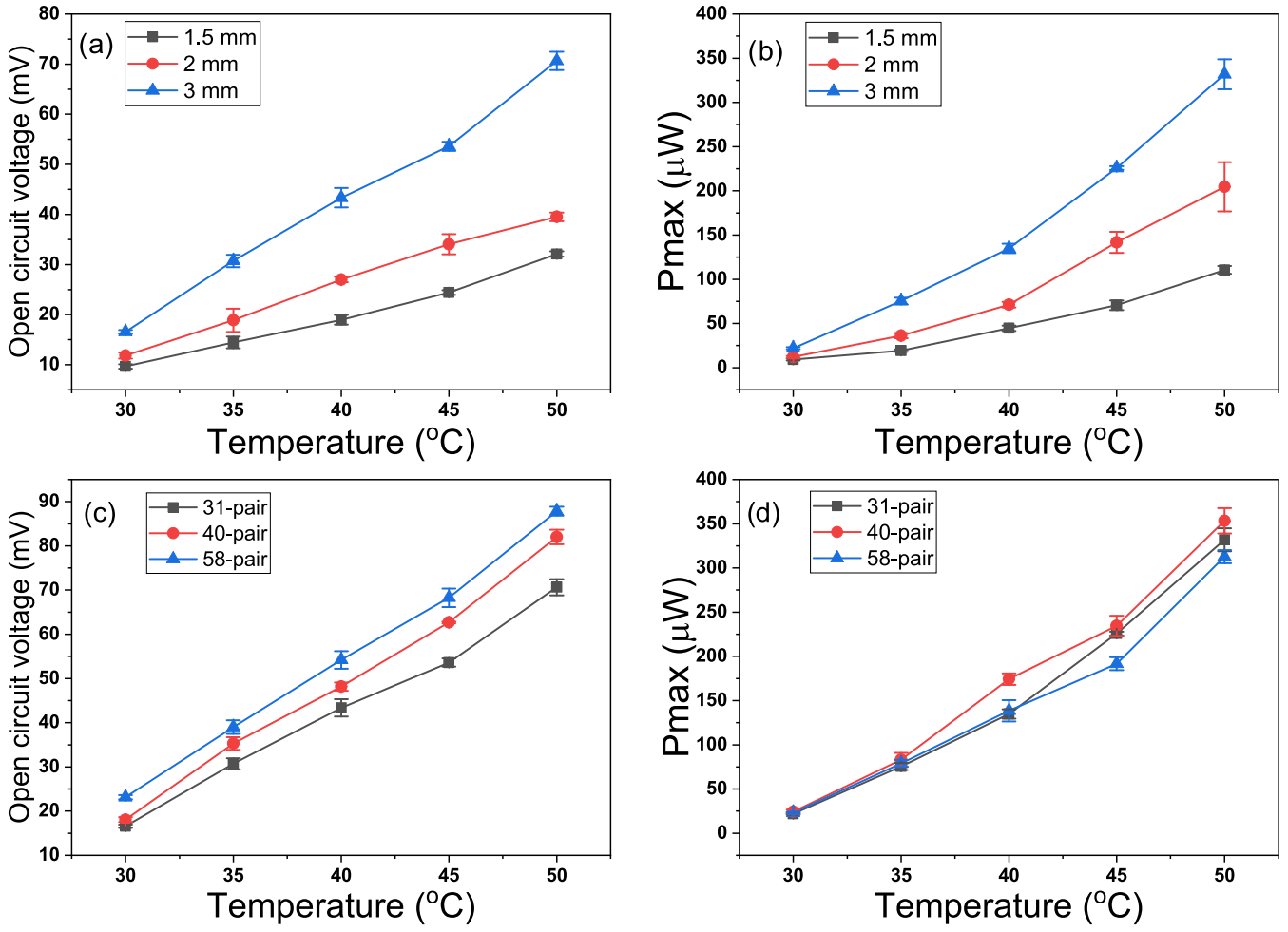

Figure 8. Curved heat source: different heights of the TE legs (31-pair) (a) open-circuit voltage, (b) maximum output power; different filling factor (3 mm leg length) (c) open-circuit voltage, (d) maximum output.

highest power because the leg length of 3 mm corresponds to the optimum FF 0.101 (40-pair).

4.2.3. Curved Heat Source. Figure 8 presents the analysis of the open-circuit voltage and the output power of the TE modules based on the curved heat source where the ambient temperature is 23 °C. Similar to Figure 7a, the open-circuit voltage in Figure 8a increases with the heat source temperature. Herein, the results also demonstrate an increase with an increase in the leg length. This occurs because the higher the leg length, the larger the temperature gradient across the two sides of the w-TEG. At the heat source temperature of 50 °C, the maximum open-circuit voltages were 32, 39.5, and 70.6 mV for the TE modules with L = 1.5, 2, and 3 mm, respectively. The output powers of the three TE modules also increase with the heat source temperature, as shown in Figure 8b. Even though the internal resistance of the TE modules increases with leg length, the output power increases with leg length. It can be observed that the differences among the output powers of the three TE modules become larger as the heat source temperature increases. This is because as the heat source temperature increases, the temperature gradient also increases. The influence of the temperature gradient on the output power is more significant at higher temperature gradients. It should be noted that a continuous increase in the leg length will not result in a continuous increase in the output power. As already seen in the theoretical results, a further increase in the internal resistance will dominate the increase in the temperature gradient, and thus, the output power will eventually decrease with a further increase in the leg length. The maximum output powers of 110.5, 204.6, and 331.9 μW were obtained for the TE modules with 31, 40, and 58 pairs, respectively.

Figure 8c,d shows the open-circuit voltage and the output power of the TE modules with a different number of thermocouples. The open-circuit voltage increases with the increase in both the number of thermocouples and the heat source temperature. At the heat source temperature of 50 °C, the maximum open-circuit voltages were 70.6, 82, and 87.9 mV for the TE modules with 31, 40, and 58 pairs, respectively. The result in Figure 8d is also similar to the result in Figure 7d. This shows that the behavior of TE modules on flat and curved heat sources would be similar provided that the experimental conditions are the same. The maximum output powers of 331.9, 353.4, and 312.8 μW were obtained for the TE modules with 31, 40, and 58 pairs, respectively. Like in Figure 7d, the 40-pair TE module in Figure 8d has the highest output power due to the reason stated earlier.

Table 3 provides a comparison of recent research studies on w-TEGs. It is evident that the normalized power density (N_p), defined as the power density per unit temperature gradient, achieved in the present study surpasses that of previous studies, demonstrating significant advancement in the current state of the art.

https://doi.org/10.1021/acsaem.4c01794
ACS Appl. Energy Mater. 2024, 7, 9315−9326

Table 3. Comparison of Studies on the w-TEG

material	temperature gradient (K)	power density (μW/cm^2)	N_p (μW/(cm^{2}K)	refs
bulk	4	13.2	3.3	35
bulk	40	418.6	10.465	6
bulk	14	287.5	20.54	36
bulk	0.89	2.28	2.56	37
polyester fabric	22	1.24×10^{-6}	5.6×10^{-8}	38
bulk	3	44.2	14.73	39
bulk	10.8	155	14.35	40
TE paint	30	1.42	0.05	41
bulk	9	228.1	25.34	this study

5. CONCLUSIONS

In this report, a theoretical analysis of wearable thermoelectric generators is presented and validated experimentally. The findings of this study can be summarized as follows:

- In the simulation, the open-circuit voltage of a TEG increases with an increase in the number of thermocouples/FF. On the other hand, the output power may either increase or decrease as the FF increases. This is because the output power strongly depends on the internal resistance and the thermal resistance of the TEG.
- The theoretical analysis reveals that the w-TEG with a leg length of 1.5 mm has an optimum FF of 0.078 (31-pair).
- The experimental results show that at a fixed temperature gradient and an FF of 0.078, both the open-circuit voltage and the power output increase with an increase in the temperature gradient. The highest power output of 1595.6 μW was observed at a temperature gradient of 9 K for the w-TEG with a leg length of 1.5 mm. Similarly, when the leg height is kept at 3 mm and the number of pairs was varied, both the open-circuit voltage and the maximum power output were found to increase proportionally with the temperature gradient. The w-TEG with the highest FF demonstrated the highest power output of 1806.5 μW at a temperature gradient of 9 K.
- For both flat and curved heat sources (50 °C) where the cold side of the TEG is cooled by natural convection, when the number of pairs is varied, the highest power output is observed at 40 pairs. This is because the temperature gradient and internal resistance change with the number of pairs, indicating that both factors must be considered to achieve an optimized thermoelectric device structure for real-world applications. Specifically, in the case of 58 pairs, nearly twice as many thermoelectric legs are used compared to 31 pairs, yet the power output is almost the same. For the 40-pair, the highest output powers of the TE module (L = 3 mm) with flat and curved heat sources were 345.9 and 353.4 μW, respectively. A similar output level was observed for both flat and curved heat sources, indicating that the fabricated w-TEG is uniformly attached and can operate reliably even in curved environments.

APPENDIX A

Error bars, indicating the standard deviation (SD), were used to represent the variability in the data in the Experimental Section. The average and standard deviation were calculated from three experiments using eqs A1 and A2.

$$x_{av} = \frac{x_1 + x_2 + x_3}{3} \tag{A.1}$$

$$SD = \sqrt{\frac{\sum_{i=1}^{3} (x_i - x_{av})^2}{3 - 1}} \tag{A.2}$$

Each data group is shown by its mean (x_{av}) and the error bars illustrate the SD for that group. The error bars reflect the spread of data points, with smaller error bars suggesting less deviation from the mean and, consequently, more reliable data.

ASSOCIATED CONTENT

Data Availability Statement

The data that support the findings of this study is available from the corresponding authors upon reasonable request.

Supporting Information

The Supporting Information is available free of charge at https://pubs.acs.org/doi/10.1021/acsaem.4c01794.

Fabrication procedure of w-TEG and thermoelectric material property data from the supplier (PDF)

AUTHOR INFORMATION

Corresponding Authors

Jeong Hun Kim − *Smart Materials Research Section, Electronics and Telecommunications Research Institute, Daejeon 305-700, Republic of Korea*; Email: jeonghun@etri.re.kr

Sedat Ballikaya − *Department of Engineering Sciences, Istanbul University−Cerrahpaşa, Istanbul 34320, Turkey*; orcid.org/0000-0002-0588-2212; Email: ballikaya@iuc.edu.tr

Authors

Aminu Yusuf − *Department of Engineering Sciences, Istanbul University−Cerrahpaşa, Istanbul 34320, Turkey*

Seung Eon Moon − *Smart Materials Research Section, Electronics and Telecommunications Research Institute, Daejeon 305-700, Republic of Korea*

Jong Pil Im − *Smart Materials Research Section, Electronics and Telecommunications Research Institute, Daejeon 305-700, Republic of Korea*

Complete contact information is available at: https://pubs.acs.org/10.1021/acsaem.4c01794

Author Contributions

J.H.K.: conceptualization, funding acquisition, supervision, experimental analysis, writing—review and editing. A.Y.: theoretical analysis, software, writing—original draft, writing—review and editing. S.E.M. and J.P.I.: methodology, investigation. S.B.: funding acquisition, supervision, writing—review and editing.

Notes

The authors declare no competing financial interest.

https://doi.org/10.1021/acsaem.4c01794
ACS Appl. Energy Mater. 2024, 7, 9315−9326

■ ACKNOWLEDGMENTS

A.Y. and J.H.K. contributed equally to this work. This work was supported by the Scientific and Technological Research Council of Turkey (TUBITAK) with project number 119N120. It also received support from an internal fund/grant of the Electronics and Telecommunications Research Institute (ETRI) (24YB1900) and the National R & D program through the National Research Foundation of Korea (NRF) funded by the Ministry of Science and ICT (NRF-2021M3C1C3097542).

■ NOMENCLATURE

Symbols

A across-sectional area (m^2)
FF fill factor
I electric current (A)
k thermal conductivity (W/(K m))
l leg length (m)
N number of thermocouples
m ratio of load and internal resistances
Q_c heat released (W)
Q_h heat absorbed (W)
R resistance (Ω)
R_{TE} thermal resistance (K/W)
S Seebeck coefficient (μV/K)
T temperature (K)
ZT device figure-of-merit (1/K)

Greek Symbols

σ electrical conductivity (S/m)
ρ density (kg/m^3)
τ Thomson coefficient (μV/K)

Subscripts

av average
c cold side
h hot side
I internal
L load
nn-type
pp-type
TE thermoelectric

■ REFERENCES

(1) Cui, Y. J.; Wang, B. L.; Wang, K. F. Energy conversion performance optimization and strength evaluation of a wearable thermoelectric generator made of a thermoelectric layer on a flexible substrate. *Energy* **2021**, *229*, No. 120694.
(2) Im, J.-P.; Kim, J.; Lee, J.; Woo, J.; Im, S.; Kim, Y.; et al. Self-Powered Autonomous Wireless Sensor Node by Using Silicon-Based 3D Thermoelectric Energy Generator for Environmental Monitoring Application. *Energies* **2020**, *13*, No. 674.
(3) Van Toan, N.; Tuoi, T. T. K.; Van Hieu, N.; Ono, T. Thermoelectric generator with a high integration density for portable and wearable self-powered electronic devices. *Energy Convers. Manage.* **2021**, *245*, No. 114571.
(4) Wen, D.-L.; Liu, X.; Bao, J.-F.; Li, G.-K.; Feng, T.; Zhang, F.; et al. Flexible Hybrid Photo-Thermoelectric Generator Based on Single Thermoelectric Effect for Simultaneously Harvesting Thermal and Radiation Energies. *ACS Appl. Mater. Interfaces* **2021**, *13*, 21401−21410.
(5) Shi, Y.; Wang, Y.; Mei, D.; Feng, B.; Chen, Z. Design and Fabrication of Wearable Thermoelectric Generator Device for Heat Harvesting. *IEEE Rob. Autom. Lett.* **2018**, *3*, 373−378.
(6) Lee, B.; Cho, H.; Park, K. T.; Kim, J.-S.; Park, M.; Kim, H.; et al. High-performance compliant thermoelectric generators with magnetically self-assembled soft heat conductors for self-powered wearable electronics. *Nat. Commun.* **2020**, *11*, No. 5948.
(7) Toan, N. V.; Tuoi, T. T. K.; Sui, H.; Trung, N. H.; Samat, K. F.; Ono, T. Ultra-flexible thermoelectric generator based on silicone rubber sheet and electrodeposited thermoelectric material for waste heat harvesting. *Energy Rep.* **2022**, *8*, 5026−5037.
(8) Feng, R.; Tang, F.; Zhang, N.; Wang, X. Flexible, High-Power Density, Wearable Thermoelectric Nanogenerator and Self-Powered Temperature Sensor. *ACS Appl. Mater. Interfaces* **2019**, *11*, 38616−38624.
(9) Karthikeyan, V.; Surjadi, J. U.; Wong, J. C. K.; Kannan, V.; Lam, K.-H.; Chen, X.; et al. Wearable and flexible thin film thermoelectric module for multi-scale energy harvesting. *J. Power Sources* **2020**, *455*, No. 227983.
(10) Wang, Y.; Shi, Y.; Mei, D.; Chen, Z. Wearable thermoelectric generator to harvest body heat for powering a miniaturized accelerometer. *Appl. Energy* **2018**, *215*, 690−698.
(11) Liu, L.; Chen, J.; Liang, L.; Deng, L.; Chen, G. A PEDOT:PSS thermoelectric fiber generator. *Nano Energy* **2022**, *102*, No. 107678.
(12) Jang, D.; Park, K. T.; Lee, S.-S.; Kim, H. Highly stretchable three-dimensional thermoelectric fabrics exploiting woven structure deformability and passivation-induced fiber elasticity. *Nano Energy* **2022**, *97*, No. 107143.
(13) Li, K.; Sun, X.; Wang, Y.; Wang, J.; Dai, X.; Li, G.; Wang, H. All-in-one single-piece flexible solar thermoelectric generator with scissored heat rectifying p-n modules. *Nano Energy* **2022**, *93*, No. 106789.
(14) Liang, J.; Zhang, X.; Wan, C. From Brittle to Ductile: A Scalable and Tailorable All-Inorganic Semiconductor Foil through a Rolling Process toward Flexible Thermoelectric Modules. *ACS Appl. Mater. Interfaces* **2022**, *14*, 52017−52024.
(15) Lee, D.; Park, W.; Kang, Y. A.; Lim, H. T.; Park, S.; Mun, Y.; et al. Substrate-Free Thermoelectric 25 μm-Thick Ag_2Se Films with High Flexibility and In-Plane *zT* of 0.5 at Room Temperature. *ACS Appl. Mater. Interfaces* **2023**, *15*, 3047−3053.
(16) Palaporn, D.; Mongkolthanaruk, W.; Faungnawakij, K.; Kurosaki, K.; Pinitsoontorn, S. Flexible Thermoelectric Paper and Its Thermoelectric Generator from Bacterial Cellulose/Ag_2Se Nanocomposites. *ACS Appl. Energy Mater.* **2022**, *5*, 3489−3501.
(17) Liao, Z.; Zhou, X.; Wei, G.; Wang, S.; Gao, C.; Wang, L. Intrinsically Self-Healable and Wearable All-Organic Thermoelectric Composite with High Electrical Conductivity for Heat Harvesting. *ACS Appl. Mater. Interfaces* **2022**, *14*, 43421−43430.
(18) You, H.; Li, Z.; Shao, Y.; Yuan, X.; Liu, W.; Tang, H.; et al. Flexible Bi2Te3-based thermoelectric generator with an ultra-high power density. *Appl. Therm. Eng.* **2022**, *202*, No. 117818.
(19) Xu, Q.; Deng, B.; Zhang, L.; Lin, S.; Han, Z.; Zhou, Q.; et al. High-performance, flexible thermoelectric generator based on bulk materials. *Cell Rep. Phys. Sci.* **2022**, *3*, No. 100780.
(20) Zhang, J.; Zhang, W.; Wei, H.; Tang, J.; Li, D.; Xu, D. Flexible micro thermoelectric generators with high power density and light weight. *Nano Energy* **2023**, *105*, No. 108023.
(21) Hasan, M. N.; Nayan, N.; Nafea, M.; Muthalif, A. G. A.; Ali, M. S. M. Novel structural design of wearable thermoelectric generator with vertically oriented thermoelements. *Energy* **2022**, *259*, No. 125032.
(22) Kuang, N.; Niu, A.; Wang, W.; Zuo, Z.; Zhan, T.; Wang, H. High performance flexible thermoelectric generator using bulk legs and integrated electrodes for human energy harvesting. *Energy Convers. Manage.* **2022**, *272*, No. 116337.
(23) Jeong, M. H.; Kim, K.; Kim, J.; Choi, K. J. Operation of Wearable Thermoelectric Generators Using Dual Sources of Heat and Light. *Adv. Sci.* **2022**, *9*, No. 2104915.
(24) Bahk, J.-H.; Fang, H.; Yazawa, K.; Shakouri, A. Flexible thermoelectric materials and device optimization for wearable energy harvesting. *J. Mater. Chem. C* **2015**, *3*, 10362−10374.
(25) Yusuf, A.; Demirci, Y.; Maras, T.; Moon, S. E.; Pil-Im, J.; Kim, J. H.; Ballikaya, S. Experimental and Theoretical Investigation of the Effect of Filler Material on the Performance of Flexible and Rigid

Thermoelectric Generators. *ACS Appl. Mater. Interfaces* **2021**, *13*, 61275−61285.
(26) Suarez, F.; Nozariasbmarz, A.; Vashaee, D.; Öztürk, M. C. Designing thermoelectric generators for self-powered wearable electronics. *Energy Environ. Sci.* **2016**, *9*, 2099−2113.
(27) Nozariasbmarz, A.; Collins, H.; Dsouza, K.; Polash, M. H.; Hosseini, M.; Hyland, M.; et al. Review of wearable thermoelectric energy harvesting: From body temperature to electronic systems. *Appl. Energy* **2020**, *258*, No. 114069.
(28) Yuan, J.; Zhu, R. A fully self-powered wearable monitoring system with systematically optimized flexible thermoelectric generator. *Appl. Energy* **2020**, *271*, No. 115250.
(29) Yusuf, A.; Bayhan, N.; Ibrahim, A. A.; Tiryaki, H.; Ballikaya, S. Geometric optimization of thermoelectric generator using genetic algorithm considering contact resistance and Thomson effect. *Int. J. Energy Res.* **2021**, *45*, 9382−9395.
(30) Pennelli, G.; Dimaggio, E.; Macucci, M. Electrical and thermal optimization of energy-conversion systems based on thermoelectric generators. *Energy* **2022**, *240*, No. 122494.
(31) Chen, Y.; Xie, C.; Li, Y.; Zhu, W.; Xu, L.; Gooi, H. B. An improved metaheuristic-based MPPT for centralized thermoelectric generation systems under dynamic temperature conditions. *Energy* **2023**, *277*, No. 127485.
(32) Yusuf, A.; Ballikaya, S. Electrical, thermomechanical and cost analyses of a low-cost thermoelectric generator. *Energy* **2022**, *241*, No. 122934.
(33) Siouane, S.; Jovanović, S.; Poure, P. Fully Electrical Modeling of Thermoelectric Generators with Contact Thermal Resistance Under Different Operating Conditions. *J. Electron. Mater.* **2017**, *46*, 40−50.
(34) Rösch, A. G.; Franke, L.; Mallick, M. M.; Lemmer, U. Optimizing printed thermoelectric generators with geometry and processibility limitations. *Energy Convers. Manage.* **2023**, *279*, No. 116776.
(35) Yang, S.; Li, Y.; Deng, L.; Tian, S.; Yao, Y.; Yang, F.; et al. Flexible thermoelectric generator and energy management electronics powered by body heat. *Microsyst. Nanoeng.* **2023**, *9*, No. 106.
(36) Fan, W.; Shen, Z.; Zhang, Q.; Liu, F.; Fu, C.; Zhu, T.; Zhao, X. High-Power-Density Wearable Thermoelectric Generators for Human Body Heat Harvesting. *ACS Appl. Mater. Interfaces* **2022**, *14*, 21224−21231.
(37) Kim, C. S.; Lee, G. S.; Choi, H.; Kim, Y. J.; Yang, H. M.; Lim, S. H.; et al. Structural design of a flexible thermoelectric power generator for wearable applications. *Appl. Energy* **2018**, *214*, 131−138.
(38) Siddique, A. R. M.; Rabari, R.; Mahmud, S.; Heyst, B. V. Thermal energy harvesting from the human body using flexible thermoelectric generator (FTEG) fabricated by a dispenser printing technique. *Energy* **2016**, *115*, 1081−1091.
(39) Nozariasbmarz, A.; Suarez, F.; Dycus, J. H.; Cabral, M. J.; LeBeau, J. M.; Öztürk, M. C.; Vashaee, D. Thermoelectric generators for wearable body heat harvesting: Material and device concurrent optimization. *Nano Energy* **2020**, *67*, No. 104265.
(40) Yusuf, A.; Demirci, Y.; Maras, T.; Moon, S. E.; Pil-Im, J.; Kim, J. H.; Ballikaya, S. Experimental and Theoretical Investigation of the Effect of Filler Material on the Performance of Flexible and Rigid Thermoelectric Generators. *ACS Appl. Mater. Interfaces* **2021**, *13*, 61275−61285.
(41) Yilmaz, M.; Yusuf, A.; Gurkan, K.; Ballikaya, S. Developing High-Performance and Low-Cost Paint Thermoelectric Materials for Low-Midtemperature Applications. *ACS Appl. Mater. Interfaces* **2024**, *16* (10), 12661−12671.

https://doi.org/10.1021/acsaem.4c01794
ACS Appl. Energy Mater. 2024, 7, 9315−9326